PERGAMON International Journal of Impact Engineering 29 (2003) 747–755

INTERNATIONAL JOURNAL OF IMPACT ENGINEERING

www.elsevier.com/locate/ijimpeng

Analytically Modeling Hypervelocity Penetration of Thick Ceramic Targets

James D. Walker

Southwest Research Institute, P. O. Drawer 28510, San Antonio, Texas 78228 USA

Abstract

Hypervelocity impact of thick ceramic targets was examined through an analytic model for penetration. Three ceramic materials (SiC, B_4C and AlN) were modeled and compared to available test data for impacts from 1.5 to 4.5 km/s. The analytic model is based on a centerline momentum balance – a method that has proven to be an effective way to produce analytic models of penetration. A number of assumptions are required to develop the analytic penetration model, including assumptions about material motion and constitutive response of the target material. The constitutive model for the failed brittle material used in the penetration model development was a Drucker-Prager yield surface with cutoff. Such a constitutive model allows pressure dependent strength for failed material, which is the type of response seen in extensively fractured ceramic. A cutoff is used since the total strength of the failed brittle material has an upper limit. The use of this constitutive model for the failed brittle material leads to an interior boundary problem within the damaged region, demarcating the region of material flow where the strength is the cutoff and the region that is controlled by the pressure dependent strength. It is shown that excellent agreement between the model and the data across the full range of penetration velocities (1.5 to 4.5 km/s) is obtained when large slopes (on the order of 2) and large cutoff values (on the order of 3 GPa) are used. (The actual values differ for each ceramic.) Excellent agreement between the analytic model and large-scale numerical simulations with exactly the same constitutive model verify that the model correctly includes the intended physics.

Keywords: Hypervelocity impact, analytic penetration models, ceramic penetration, Drucker-Prager yield surface, silicon carbide, boron carbide, aluminum nitride.

1. Introduction

In the previous decade, a technique was introduced that gives remarkably good results in modeling projectile penetration of targets. The technique is to integrate the momentum balance along the centerline. Velocity profiles are assumed in both the target and the projectile to carry out the integration. To determine the shear stress response required in the integral, it is necessary to assume a constitutive model for the target material and a three-dimensional velocity field within the target. This technique was first applied to metal targets being penetrated by long rods [1], and has subsequently been successfully applied to thick ceramic targets [2-5], to thin

0734-743X/$ - see front matter © 2003 Elsevier Ltd. All rights reserved.
doi:10.1016/j.ijimpeng.2003.10.021

targets comprised of thin ceramic tiles backed by thin substrates [6], and to bulge and breakout of metal targets [7]. The model for thick ceramic targets gives excellent results, so far having been applied to (and matching) penetration velocity for three ceramics: SiC, B_4C and AlN.

2. The Analytic Model

Details of the model and its development can be found in previous publications [2-5]. In this paper, the concepts of the model are outlined and then the behavior of the model is examined in some detail. The model uses a centerline momentum balance, where the target and impact geometry are assumed axisymmetric with the axis of symmetry being the z axis. The target is assumed semi-infinite. The projectile lies along the z axis. The length of the projectile is denoted L. The velocity along the centerline in the projectile and target is written $u_z(z)$. The interface velocity is u and the velocity of the back of the projectile is v.

A central theme of the modeling approach is the use of the momentum balance along the z axis. On the axis itself, where $x = y = 0$, $u_x = u_y = 0$ by symmetry. Since the x and y directions are equivalent, the momentum balance along the centerline simplifies to, where ρ is the density and σ_{ij} the appropriate stress tensor term:

$$\rho\frac{\partial u_z}{\partial t}+\frac{1}{2}\rho\frac{\partial (u_z)^2}{\partial z}-\frac{\partial \sigma_{zz}}{\partial z}-2\frac{\partial \sigma_{xz}}{\partial x}=0 \tag{1}$$

The following assumptions are made based on the examination of large-scale numerical (hydrocode) simulations of long-rod impacts performed for numerous impact simulations at different impact velocities and with various materials:

1) A velocity profile along the centerline in both projectile and target is specified;
2) The back end of the projectile is decelerated by elastic waves, with a magnitude proportional to the flow stress of the projectile;
3) A shear behavior in the target material is specified. This requires knowledge of the three-dimensional flow field in the target in the vicinity of the centerline so that the derivative of the shear stress can be calculated (the $\partial\sigma_{xz}/\partial x$ term in Eq. (1)). The model assumes a hemispherical flow of target material as the projectile penetrates.

With suitable expressions resulting from assumptions 1 and 3, the axial momentum equation can then be integrated to obtain an equation of motion for the location of the interface between the target and the projectile. Assumption 2 provides an equation for the deceleration of the rear of the projectile.

Initial conditions for the model include an initial interface velocity and an expression that relates the crater radius to the impact velocity. The first is obtained from the equations for one-dimensional plate impact (the particle velocity in the Rankine-Hugoniot relations). A cavity expansion solution is used to estimate the extent of plastic flow within the target.

3. The Constitutive Model

It is assumed that the ceramic can be modeled with a Drucker-Prager constitutive model, or yield surface, with cutoff:

$$Y=\begin{cases} Y_0+bp, & p<(\overline{Y}-Y_0)/b \\ \overline{Y}, & p>(\overline{Y}-Y_0)/b \end{cases} \tag{2}$$

where Y is the flow stress, p is the pressure, and $\bar{Y}$ is a maximal flow stress (Fig. 1). This pressure dependent yield is given by a zero pressure flow stress Y_0 and a slope b. The von Mises flow surface can be viewed as a special case of Eq. (2), with $b = 0$.

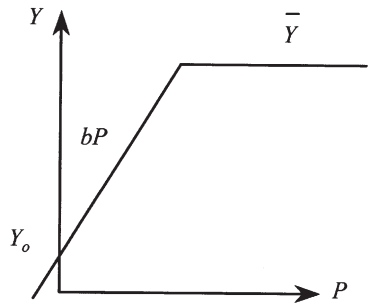

Fig. 1. Drucker-Prager constitutive model.

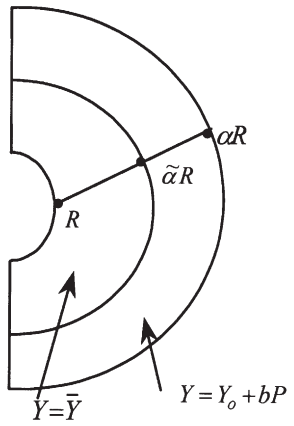

Fig. 2. Target geometry.

For the penetration problem where the target response is modeled with a Drucker-Prager yield criterion with cutoff, the target response is broken into two regions. Near the projectile target interface, the stresses are high, and the flow stress is given by the cutoff value $\bar{Y}$. Further away from the projectile-target interface, stresses and pressures decrease and the flow stress of the target material is modeled by the pressure dependent response $Y_0 + bp$. Geometrically, due to the assumption of a hemispherical flow field in the target, the region where the flow stress equals the cutoff $\bar{Y}$ ranges from the crater radius R to an intermediate radius $\tilde{\alpha}R$ (Fig. 2). The pressure dependent portion of the flow surface then ranges from this intermediate radius $\tilde{\alpha}R$ to the outer edge αR.

4. The Analytic Model

The integral of the centerline momentum balance within the two regions in the target is combined with the projectile centerline momentum balance to give:

$$\begin{aligned}
&\rho_p \dot{v}(L-s)+\dot{u}\left[\rho_p s+\frac{\rho_p\alpha^2 s^2}{(\alpha^2-1)R}+\frac{\rho_t R}{\alpha^2-1}\left\{\alpha^2-\frac{\alpha^2}{\tilde{\alpha}}-\tilde{\alpha}+1+\frac{1}{\tilde{\alpha}^\delta}\left(\alpha^2\frac{\alpha^{\delta-1}-\tilde{\alpha}^{\delta-1}}{\delta-1}-\frac{\alpha^{\delta+1}-\tilde{\alpha}^{\delta+1}}{\delta+1}\right)\right\}\right]\\
&\quad=\frac{1}{2}\rho_p(v-u)^2-\frac{7}{3}\bar{Y}\ln(\tilde{\alpha})-\frac{Y_0}{b}\left\{\left(\frac{\alpha}{\tilde{\alpha}}\right)^\delta-1\right\}-\frac{1}{2}\rho_t u^2\left(\frac{\alpha}{\tilde{\alpha}}\right)^4\left(\frac{\tilde{\alpha}^2-1}{\alpha^2-1}\right)^2\\
&\quad-\frac{2\rho_t\alpha^4u^2}{\tilde{\alpha}^\delta(\alpha^2-1)^2}\left\{\frac{\alpha^{\delta-2}-\tilde{\alpha}^{\delta-2}}{\delta-2}-\frac{\alpha^{\delta-4}-\tilde{\alpha}^{\delta-4}}{\delta-4}\right\}\\
&\quad-\frac{2u\alpha\dot{\alpha}}{(\alpha^2-1)^2}\left[\frac{\rho_t R}{\tilde{\alpha}}(\tilde{\alpha}-1)^2-\frac{\rho_p s^2}{R}+\frac{\rho_t R}{\tilde{\alpha}^\delta}\left\{\frac{\alpha^{\delta+1}-\tilde{\alpha}^{\delta+1}}{\delta+1}-\frac{\alpha^{\delta-1}-\tilde{\alpha}^{\delta-1}}{\delta-1}\right\}\right]
\end{aligned}\tag{3}$$

where $\delta = 7b/(3+2b)$, s is the extent of the plastic zone in the projectile (it is related to R), and the dots refer to differentiation with respect to time. Additional equations give the deceleration of the tail of the projectile based on elastic waves traveling the length of the projectile and reflecting off the free surface, and the time rate of change of the length of the projectile as the difference between the penetration speed and the speed of the tail.

To get a better understanding of the physics in Eq. (3), if the parameters that were introduced that include the three-dimensional model geometry (R and s) are allowed to go to zero, then, using the deceleration equation for the rear of the projectile ($\rho_p L\dot{v} = -Y_p$), it can be shown that Eq. (3) reduces to Tate's formulation. For example, in the case where the whole deforming region in the target is plastically flowing at the cutoff stress $\bar{Y}$ ($\tilde{\alpha} \equiv \alpha$), the resulting target resistance term is $R_t = (7/3)\bar{Y}\ln(\alpha)$. For the more complicated case when the whole region is flowing with a pressure-dependent stress ($\tilde{\alpha} \equiv 1$),

$$R_t = \frac{Y_0}{b}\{\alpha^{\delta} - 1\} + \rho_t u^2 \left[\frac{2\alpha^4}{(\alpha^2-1)^2}\left\{\frac{\alpha^{\delta-2}-1}{\delta-2} - \frac{\alpha^{\delta-4}-1}{\delta-4}\right\} - \frac{1}{2}\right] \tag{4}$$

Thus, the target resistance is a function of the penetration velocity squared, as would be expected since it is a function of pressure ($p \sim \frac{1}{2}\rho_t u^2$). The term in square brackets on the right hand side shows a rough linear dependence on b. It also depends on velocity, since α is a function of penetration velocity. Figure 3 shows the term in square brackets as a function of b for α computed for three penetration velocities using the constants for SiC presented below. It is seen that as the penetration velocity increases, the term in square brackets decreases. Thus, overall, the second expression on the right hand side of Eq. (4) roughly depends linearly on b and depends somewhere between linearly and squared on the penetration velocity. If the limit $b \to 0$ is taken, the result is $R_t = (7/3)Y_0 \ln(\alpha)$ – the whole region is flowing with a flow stress of Y_0.

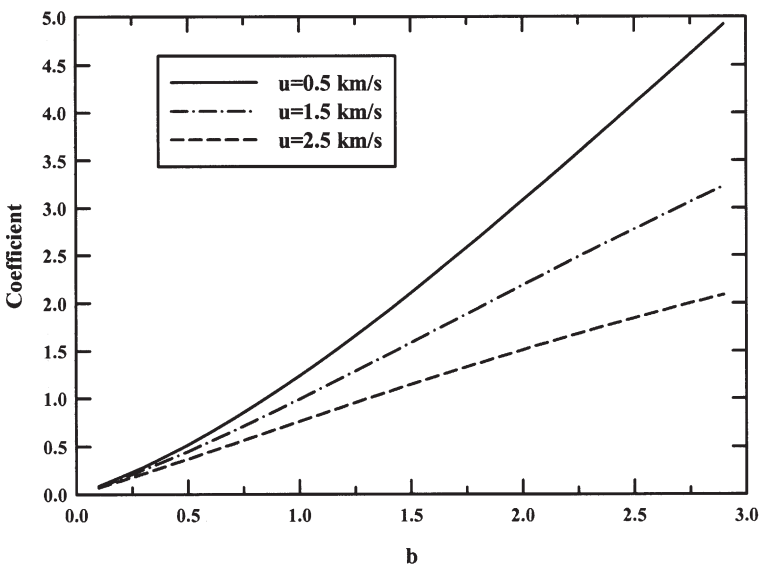

Fig. 3. Coefficient in Eq. (4).

In using Eq. (3) to compute the front and tail velocity of the projectile, it is necessary to solve for the interior boundary $\tilde{\alpha}$. At this boundary, the axial stress deviator is assumed continuous. This condition in practice leads to a nonlinear equation for $\tilde{\alpha}$ that must be solved simultaneously with Eq. (3) and the projectile rear deceleration equation (the other two unknowns are $\dot{u}$ and $\dot{v}$). In the work reported here, this solution was found with an iterative quasi-Newton procedure. As a first step, however, one solves the problem without cutoff ($\tilde{\alpha} = 1$) to see if the stresses are such that the cutoff is even reached.

The calculation of α, the outer radius of the flow field, is through a cavity expansion solution based on the intact material's bulk modulus and a flow stress Y_{cav} [1]. The crater radius is taken to depend on the projectile radius and the impact velocity (hence, the crater radius is constant throughout the penetration). The equation used is a fit to data of tungsten long rods into steel targets that depends quadratically on the impact velocity. It has proven to work for many different materials [1].

5. Silicon Carbide

As an example of the above model, the penetration of SiC by a tungsten long-rod projectile will be considered. The experimental work in [8] is for a L/D=20 tungsten projectile being impacted by a SiC target. For modeling purposes, the projectile density was assumed 19.3 g/cm^3, bar wave speed 5.0 km/s, and flow stress (Y_p) 2.0 GPa. The properties for the SiC were density 3.22 g/cm^3, bulk modulus (K) 230 GPa, shear modulus (G) 180 GPa, bulk sound speed 8.48 km/s and a slope for the u_s-u_p curve of 1.0 [9]. There are four available numbers for the ceramic to be used in fitting the penetration data: the three values for the Drucker-Prager flow stress with cutoff (Y_0, b, $\bar{Y}$), and the strength of the target Y_{cav} required for the cavity expansion calculation of α. For the latter, it was assumed that the appropriate flow stress for the extent of the flowing region would be based on an average of the cutoff strength and the zero pressure strength, since it is known that the actual stress will be between those values. Thus, it was assumed that $Y_{cav} = (Y_0 + \bar{Y})/2$. This leaves three variables to fit the data.

The choice was to make the fit to the penetration velocity vs. impact velocity data. The best fit was achieved with values Y_0 = 0.1 GPa, b = 2.5, and $\bar{Y}$ = 3.7 GPa. In the analytic model, an average penetration velocity for each impact velocity was calculated by fitting a least squares line through the three depth of penetration vs. time points when the projectile had eroded 1/4, 1/2, and 3/4 of its initial length and through the zero time-zero penetration point, as done in [8]. Using the above constants, the analytic model gives penetration velocity versus time as plotted in Fig. 4. The agreement is remarkable. Also on the plot are the least squares line obtained experimentally (it is nearly completely covered by the model curve) and the "hydrodynamic" line for comparison – the theoretical penetration velocity if the ceramic and projectile had no strength.

In addition, Fig. 4 contains computational points where large-scale numerical simulations were run with the hydrocode CTH [10] with the identical constitutive model (Eq. 2) and material constants and parameters as in the analytic model. A zoning of 10 computational cells across the radius of the projectile was used. Agreement between the hydrocode and analytic model computations is excellent, verifying that the analytic model is correctly reflecting the physics of the penetration event given the pressure-dependent constitutive model.

Figure 5 displays the final depth of penetration of the model versus that seen in the experiments. The agreement is good. Also included on the plot is the hydrodynamic line, showing that the ceramic as an armor does considerably better than hydrodynamic for impact velocities of 2 – 3 km/s. Figure 5 also displays the results of the CTH computations, and again, agreement is good. Figure 6 displays α and $\tilde{\alpha}$ for each impact velocity at the point in penetration when 1/2 of the projectile is eroded. The decrease in α reflects the compressibility of the material at the higher impact velocities, and the slow growth in $\tilde{\alpha}$ shows the region where the flowing target material has the $\bar{Y}$ cutoff flow stress, which ranges from 3% of the flowing region by radius at 1 km/s to 67% by radius at 5 km/s.

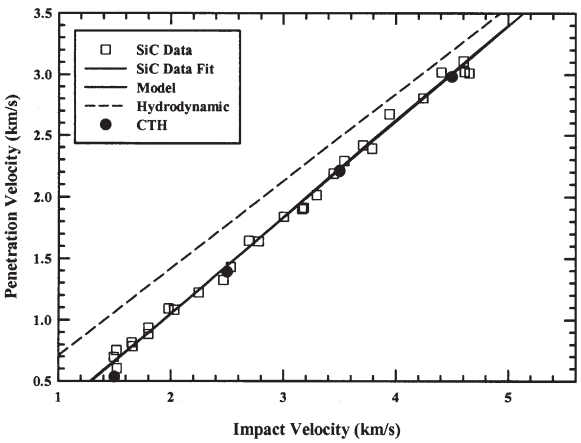

Fig. 4. Penetration velocity vs. impact velocity for both the model and experimental data for tungsten into SiC.

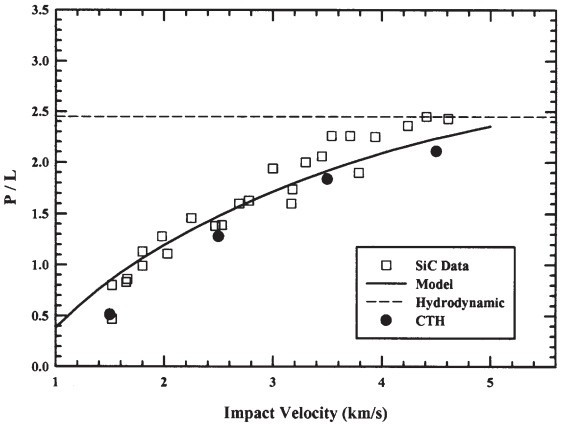

Fig. 5. Penetration versus impact velocity for both the model and experimental data for tungsten into SiC.

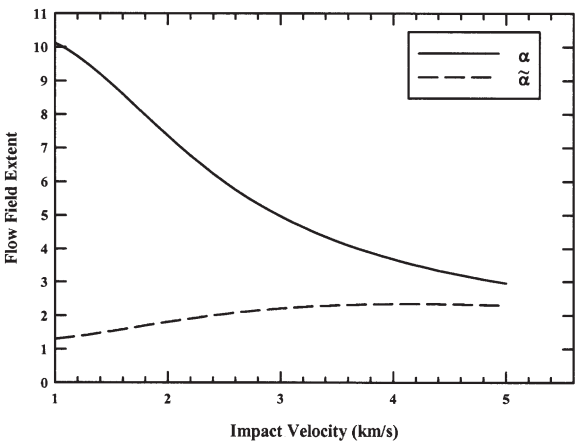

Fig. 6. Extents of the flow regions vs. impact velocity for model.

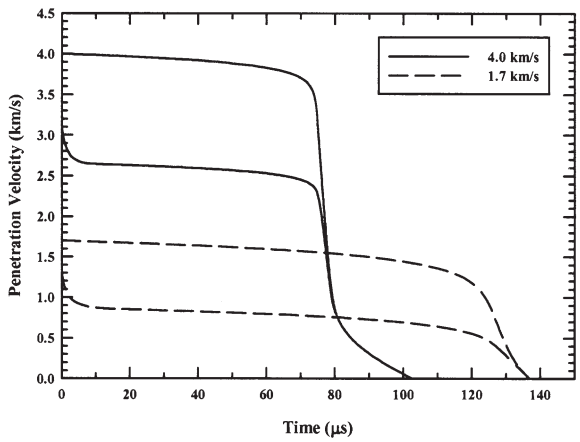

Fig. 7. Penetration and tail velocities versus time for two impact velocities.

Figure 7 displays the penetration and tail velocities versus time for two impact velocities: 1.7 km/s and 4.0 km/s. The majority of the penetration is at relatively steady-state velocities, but of particular interest here are the relatively long "tails" at the end of penetration, where the small residual length of the projectile is penetrating into fracture ceramic material.

6. Boron Carbide

Next, the penetration of B_4C by a tungsten long-rod projectile is considered. The experimental work in [11] is for a L/D=20 tungsten projectile being impacted by a B_4C target. For modeling purposes, again the projectile density was assumed 19.3 g/cm^3, bar wave speed 5.0 km/s, and flow stress (Y_p) 2.0 GPa. The properties for the B_4C were density 2.50 g/cm^3, bulk modulus (K) 232 GPa, shear modulus (G) 198 GPa, bulk sound speed 8.885 km/s and a slope for the u_s-u_p curve of 1.0 [9]. Again, it was assumed that $Y_{cav} = (Y_0 + \bar{Y})/2$.

The parameters were adjusted to fit the penetration velocity vs. impact velocity data, as described above. The best fit was achieved with values $Y_0 = 0.1$ GPa, $b = 1.7$, and $\bar{Y} = 4.0$ GPa. The penetration velocities, with the above constants, versus time are plotted in Fig. 8. The

agreement is very good. Also on the plot is the least squares line obtained experimentally. For B_4C, the analytic model calculation is slightly above the least squares line fit at higher velocities. The "hydrodynamic" line is included for comparison – the theoretical penetration velocity if the ceramic and projectile had no strength.

Figure 9 displays the final depth of penetration of the model versus that seen in the experiments. The model prediction falls below the experimental data. Since the model predicts a slightly higher penetration velocity at higher velocities, it must be that the difference in the final penetration depths arises at late time, during the tail of penetration. Figure 10 displays α and $\tilde{\alpha}$ for each impact velocity at the point in penetration when 1/2 of the projectile is eroded. The $\bar{Y}$ cutoff flow stress region ranges from none of the flowing region at 1 km/s to 53% by radius at 5 km/s. Figure 11 displays the penetration and tail velocities versus time for two impact velocities: 1.7 km/s and 4.0 km/s.

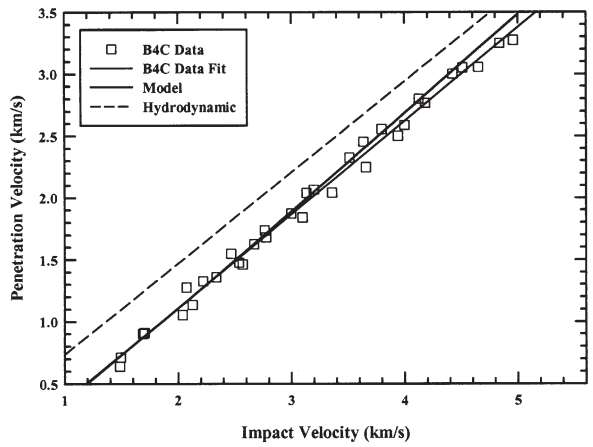

Fig. 8. Penetration velocity vs. impact velocity for both the model and experimental data for tungsten into B_4C.

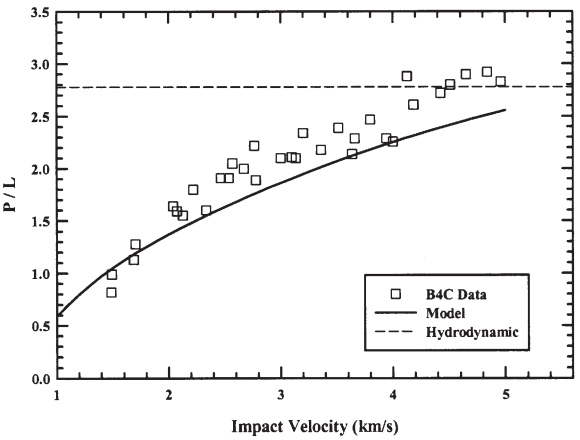

Fig. 9. Penetration versus impact velocity for both the model and experimental data for tungsten into B_4C.

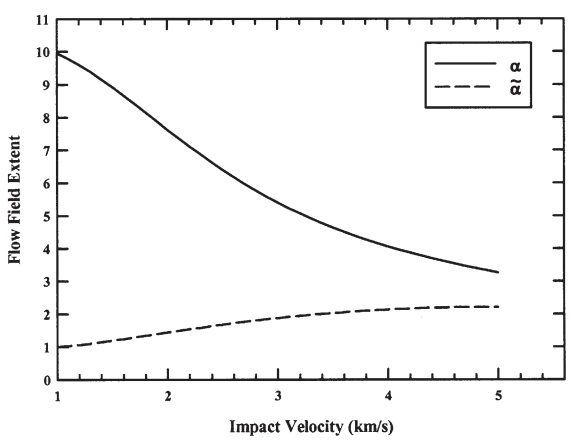

Fig. 10. Extents of the flow regions vs. impact velocity for model.

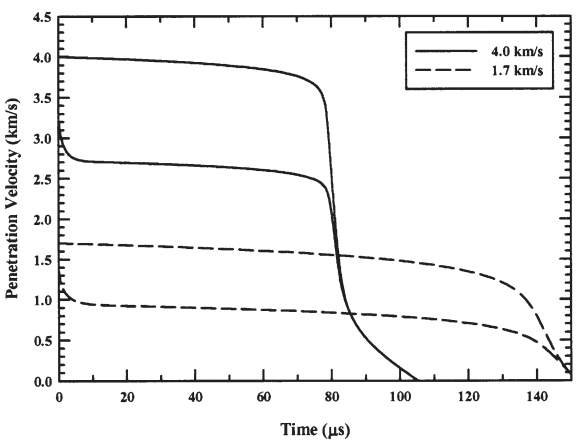

Fig. 11. Penetration and tail velocities versus time for two impact velocities.

7. Aluminum Nitride

Next, the penetration of AlN by a tungsten long-rod projectile is considered. The experimental work in [12] is for a L/D=20 tungsten projectile being impacted by a AlN target. For modeling purposes, the projectile density was assumed 19.3 g/cm^3, bar wave speed 5.0 km/s, and flow stress (Y_p) 2.0 GPa (again, the same as above). The properties for the AlN were density 3.25 g/cm^3, bulk modulus (K) 320 GPa, shear modulus (G) 129 GPa, bulk sound speed 7.90 km/s and a slope for the u_s-u_p curve of 1.0 [9]. Again, it was assumed that $Y_{cav} = (Y_0 + \overline{Y})/2$.

The parameters were adjusted to fit the penetration velocity vs. impact velocity data, as described above. The best fit was achieved with values $Y_0 = 0.1$ GPa, $b = 2.7$, and $\overline{Y} = 3.0$ GPa. The penetration velocities, with the above constants, versus time are plotted in Fig. 12. The agreement is again remarkable. The plot includes plot the least squares line obtained experimentally (nearly completely covered by the model curve) and the "hydrodynamic" line.

Figure 13 displays the final depth of penetration of the model versus that seen in the experiments. The agreement is good, though at higher velocities the predicted depth is again low. Figure 14 displays α and $\tilde{\alpha}$ for each impact velocity at the point in penetration when 1/2 of the projectile is eroded. The $\overline{Y}$ cutoff flow stress region ranges from 6% of the flowing region by radius at 1 km/s to 67% by radius at 5 km/s. Figure 15 displays the penetration and tail velocities versus time for the two impact velocities 1.7 km/s and 4.0 km/s.

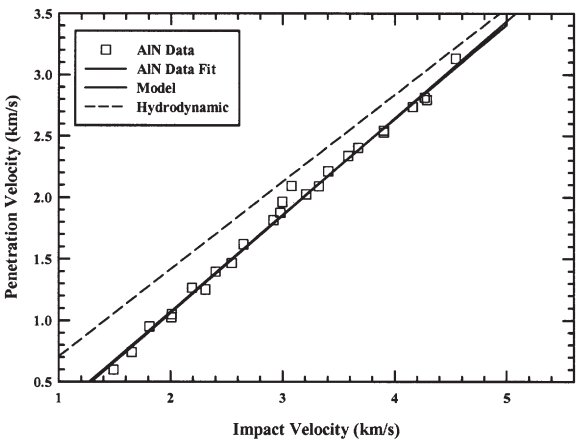

Fig. 12. Penetration velocity vs. impact velocity for the model and experimental data for tungsten into AlN.

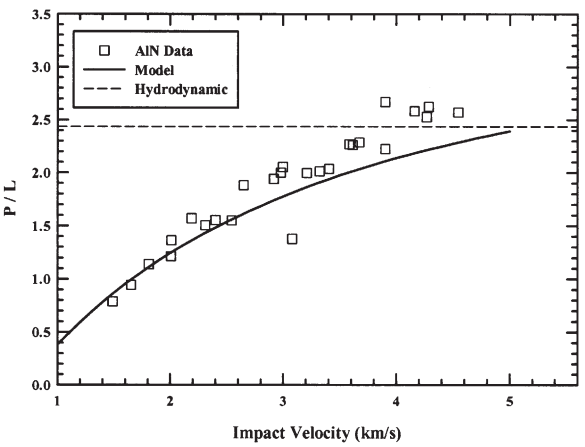

Fig. 13. Penetration versus impact velocity for both the model and experimental data for tungsten into AlN.

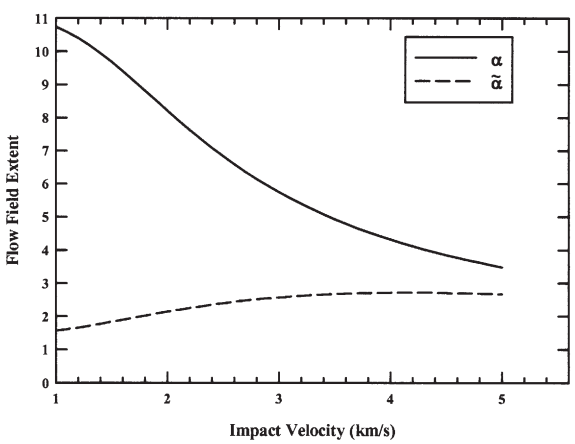

Fig. 14. Extents of the flow regions vs. impact velocity for model.

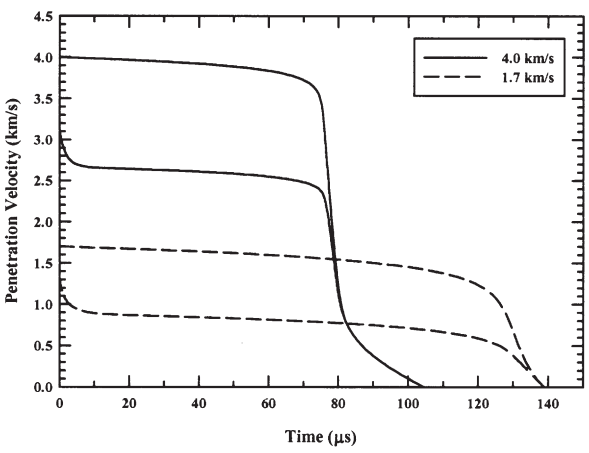

Fig. 15. Penetration and tail velocities versus time for two impact velocities.

8. Summary

This paper presented the approach of looking at a centerline momentum balance to analyze penetration. Models based on this technique include transient effects. The model has been explicitly formulated for pressure-dependent yield stress, in particular a Drucker-Prager constitutive model with a cutoff. The model shows remarkable agreement for penetration of thick ceramic targets for velocities ranging from 1.5 to 5.0 km/s. The model was compared in detail with test data from SiC, B_4C and AlN. Excellent agreement with experimental results was obtained. The model was also compared with CTH computations with exactly the same constitutive model and again the agreement was excellent, verifying that the model correctly includes the intended physics. The pressure-dependent model requires the calculation of an internal boundary in the target, demarcating the domains of the target corresponding to the cutoff flow stress and the pressure-dependent flow stress. The results are important in that they demonstrate that a complicated constitutive model can be solved analytically within the framework of a first-principles-based penetration model and for the fact that it is possible to model the penetration results for thick ceramics with such a constitutive model.

Acknowledgements

The author thanks Dennis Orphal and Charles Anderson for discussion and T. R. Sharron for assistance with figures.

References

[1] Walker JD, Anderson Jr. CE. A time-dependent model for long-rod penetration. *Int. J. Impact Engng,* 1995; **16**(1): 19-48.

[2] Littlefield DL, Anderson Jr. CE, Skaggs SR. Analysis of penetration of steel and Al_2O_3 targets. *High Pressure Science and Technology - 1993*, Schmidt SC, Shaner JW, Samara GA, Ross M., eds. New York: American Institute of Physics, 1993; **2**: 1793-1796.

[3] Walker JD, Anderson Jr. CE. An analytical penetration model for a drucker-prager yield surface with cutoff. *Shock Compression of Condensed Matter - 1997*, Schmidt SC, Dandekar DP, Forbes JW, eds. New York: American Institute of Physics, 1997. p. 897-900.

[4] Walker JD, Anderson Jr. CE. Penetration modeling of ceramic and metal targets. AIAA Paper #98-0829, 36th Aerospace Sciences Meeting, Reno, NV, January 1998.

[5] Walker JD. Analytic model for penetration of thick ceramic targets. *Ceramic Armor Materials by Design*, Ceramic Transactions Vol. 134, Ed. JW McAuley, *et al.*, American Ceramics Society, 2001. p. 337-348.

[6] Walker JD, Anderson Jr. CE. An analytical model for ceramic faced light armors. *Proceedings, 16th International Symposium on Ballistics*, Virginia: ADPA, 1996; **3**: 289-298.

[7] Walker JD. An analytical velocity field for back surface bulging. *Proceedings, 18th International Symposium on Ballistics*, Pennsylvania: Technomic, 1999; **2**: 1239-1246.

[8] Orphal DL, Franzen RR. Penetration of confined silicon carbide targets by tungsten long rods at impact velocities from 1.5 to 4.6 km/s. *Int. J. Impact Engng*, 1997; **19**(1): 1-13.

[9] Holmquist TJ, Rajendran AM, Templeton DW, Bishnoi KD. A ceramic armor material database. TARDEC Technical Report #13754, U.S. Army Tank-Automotive Research, Development and Engineering Center, Detroit, MI., 1999.

[10] McGlaun JM, Thompson SL, Elrick MG. CTH: A three-dimensional shock wave physics code. *Int. J. Impact Engng,* 1990; **10**: 351-360.

[11] Orphal DL, Franzen RR, Charters AC, Menna TL, Piekutowski AJ. Penetration of confined boron carbide targets by tungsten long rods at impact velocities from 1.5 to 5.0 km/s. *Int. J. Impact Engng,* 1997; **19**(1): 15-29.

[12] Orphal DL, Franzen RR, Piekutowski AJ, Forrestal MJ. Penetration of confined aluminum nitride targets by tungsten long rods at impact velocities from 1.5 to 4.5 km/s. *Int. J. Impact Engng*, 1996; **18**(4): 355-368.